Ferroelectrics, 361:92–104, 2007
Copyright © Taylor & Francis Group, LLC
ISSN: 0015-0193 print / 1563-5112 online
DOI: 10.1080/00150190701729482

Taylor & Francis
Taylor & Francis Group

Photoacoustic and Dielectric Study of Lead Zirconate Titanate Nanoparticles

A. FERNÁNDEZ-OSORIO,[1] R. CASTAÑEDA-GUZMÁN,[2,*]
A. VÁZQUEZ-OLMOS,[2] AND ALFONSO HUANOSTA-TERA[3]

[1]Facultad de Estudios Superiores Cuautitlán, Universidad Nacional Autónoma de México. Cuautitlán Izcalli, Edo de Méx., C.P. 54740, México
[2]Centro de Ciencias Aplicadas y Desarrollo Tecnológico, Universidad Nacional Autónoma de México, México D.F., Coyoacán 04510, México
[3]Instituto de Investigaciones en Materiales, Universidad Nacional Autónoma de México, México D.F., Coyoacán 04510, México

Using Sol-Gel method lead titanate zirconate (PZT) nanoparticles with an average size of 13.07 ± 2.8 nm, estimated from transmission electron microscopy (TEM) images, were obtained. Their X-ray powder diffraction (XRD) pattern shows a single phase of $Pb(Zr_{0.52}Ti_{0.48})O_3$ nanocrystallites. Photoacoustic and dielectric experiments on these PZT nanoparticles were performed in a wide temperature range; from room temperature up to 660°C. Photoacoustic experiments performed in as synthesized powders reveal an extraordinary dispersion in a large temperature interval, attributable to the size of the PZT-nanoparticles. Combining photoacoustic and dielectric results, obtained from sintered samples it was possible to establish the existence of a dispersive ferro-paraelectric transition temperature at around 470°C. Impedance curves were used to extract both frequency dependent ($\varepsilon'(\omega)$) and frequency independent (ε') dielectric constant. The temperature dependence of (ε'), behaves in a quite dispersive manner, although a peak around 470°C is suggested. A much more elaborate situation is found when ($\varepsilon'(\omega)$) is plotted against temperature. At selected temperatures, frequency dependent curves of $\varepsilon'(\omega)$ show that at low frequencies (<100 Hz) there is a strong dispersion, but as the frequency increases $\varepsilon'(\omega)$ tends to be frequency independent. The magnitude of $\varepsilon'(\omega)$ depends slightly on the temperature.

Keywords Photoacoustics; PZT; nanoparticles; sol-gel

1. Introduction

Recently, research interests have been focused on the preparation of nanocrystalline materials [1, 2] due to their unique chemical and physical properties. The effect of size on the properties has attracted great attention; the nanostructured materials show promising applications in designing novel nanoscale devices.

Lead zirconate titanate $Pb(Zr_{1-x}\ Ti_x)O_3$ solid solutions (PZT) are ferroelectric ceramic materials with perovskite structure which have important practical applications in piezoelectric devices, ferroelectric memories, high-value capacitors and infrared pyroelectric detectors [3–5].

Received March 8, 2007.
*Corresponding author. E-mail: rosalba.castaneda@ccadet.unam.mx

In this work Pb $(Zr_{0.52}Ti_{0.48})O_3$ nanoparticles were obtained by sol-gel method starting from titanium and zirconium alkoxides and lead acetate. The first sol-gel techniques for producing PZT were reported in the mid 1980s [6, 7], although nanostructured PZT synthesized by this method have been scarcely reported [8–10]. The grain size effects in ferroelectric properties are well known to play an important role. It has been reported that PZT thin films that consist of large grains has large dielectric permittivity and large remanent polarization [11, 12]. Therefore, one of the interesting issues is to evaluate the ferroelectric properties of the nanocrystalline PZT. Since microelectronic devices are continuously scaled down, it is necessary to understand the role of nanoparticles to provide a tool to interpret ferroelectric properties on a nanoscale. Nanometer sized PZT with notable increases in surface area and greatly reduced size are expected to display better performance in these aspects of applications.

The temperature of a ferro-paraelectric transition can be determined by different techniques, such as the temperature dependence of compressibility, the permittivity behaviour, or others. Recently we have combined temperature dependent photoacoustic and dielectric experiments to investigate solid state properties that involve phase transitions and charge carrier transport [13]. If we send a laser pulse on to a material, the laser energy will be absorbed giving rise to a pressure wave which travels through this material. In a crystal, the wave pressure activates stress and strain in the lattice of a magnitude large enough to affect the compressibility of the material. This also determines the temporal profile of the coming out acoustic pressure. Therefore, registration of sound generated by a material illuminated by a laser pulse and immersed in a temperature field can reveal the characteristic temperature of a ferro-paraelectric transition. To measure the dielectric characteristics, in a relatively large temperature interval (up to 660°C), of the nanostructured synthesized materials we have performed photoacoustic experiments, accompanied by ac measurements.

2. Experimental

2.1. Synthesis

Lead acetate trihydrate, $Pb(CH_3COO)_2{\cdot}3H2O$ (99% Aldrich), titanium isopropoxide, $Ti(OCH(CH_3)_2)_4$ (99.8% Aldrich) and zirconium propoxide, $Zr(OCH_2CH_2CH_3)_4$ (99.8% Aldrich) were used to obtain $Pb(Zr_{0.52}Ti_{0.48})O_3$ nanoparticles. 10 mL of 0.4 M solutions of titanium isopropoxide $Ti[(OCH\ (CH_3)_2]_4$ and zirconium propoxide $Zr(OCH_2CH_2CH_3)_4$ in 2 metoxi ethanol, were prepared. The solutions were mixed and stirred for 30 min. On the other hand, 5.23 g of lead acetate trihydrate $Pb(CH_3COO)_2{\cdot}3H_2O$ was dissolved in 20 ml of 2 metoxi ethanol, and added to previous solution, stirring for 30 min. After this time, the pH value was adjusted to 6.5 ± 0.5, by adding 1.2 ml of distilled water, obtaining a white gel. The gel was dried at 60°C for 24 h, and then calcined at 650°C for 1 h. Finally, pale yellow PZT powder was obtained.

2.2. Structural Characterization

X-ray diffraction pattern was measured in a D5000 Siemens equipment using Cu Kα radiation ($\lambda = 1.5406$Å). High-resolution transmission electron microphotographs (HR-TEM) were obtained in a JEOL FEG2010 FASTEM analytical microscope, operating at 200 kV, by deposition of a drop of the powdered PZT methanol dispersion onto 200 mesh Cu grids coated with a carbon/collodion layer. Transmission electron microphotographs (TEM) were

obtained in a JEOL 1200EXII instrument, operating at 90 kV, by direct immersion of the grid into PZT powder, without the use of any solvent. The particle size distribution was determined from digitalized amplified micrographs by averaging the diameter measured in each particle.

2.3. Photoacoustic Experiments

The photoacoustic experiments were performed in similar way as in previous investigations [13–16]. The beam source was provided by a pulsed Nd:YAG laser (10 Hz, 5ns pulse width). Other components of the total set up are: a beam splitter, a pyroelectric detector and a piezoelectric ceramic. This last coupled to the sample through a quartz bar, as described elsewhere [16]. The averaged generated signals (300 scans) were monitored with a digital oscilloscope. Heating was realized in a well controlled electrical tubular furnace.

2.4. Dielectric Determinations

In order to carry out the dielectric property measurements a flat specimen was used, with approximate dimensions 1.5 × 4.3 × 5 mm. The ceramic sample was sintered in an air atmosphere applying 5 Ton/cm^2, and then maintaining the sample at a constant temperature (800°C) for 23 h. The relatively low sintering temperature used was to avoid grain growth because of the thermal treatment. Air drying silver conductive paint (from STRUCTURE PROBE, INC) was applied to the parallel faces to obtain a two-probe configuration, which was placed inside a well controlled (±2°C) electrical furnace. Using a Hewlett Packard 4192A Impedance Analyzer, data was collected over the frequency range 5 Hz to 13 MHz, under an applied voltage of 1 V. In order to allow thermal equilibrium, the sample was left at the preset temperature for at least 60 min between measurements. The data set consists of the real and imaginary parts of the impedance as frequency-dependent values. Experiments were performed from room temperature up to 660°C.

3. Results and Discussion

3.1. Crystallographic Features

X-ray diffraction pattern is shown in the fig. 1. This pattern reveals the formation of a single phase of a nanocrystalline product, which was identified as that of the perovskite structure of $Pb(Zr_{0.52}Ti_{0.48})O_3$. All diffraction peaks can be perfectly indexed to the tetragonal structure (JCPDS card 33-0784), these results are consistent with those reported in the literature for this composition. In order to determine the average crystallite size, a peak broadening method was applied using the classical Scherrer-Warren equation over the [1 1 1] and [2 0 0] reflections, resulting in average size of 16.3 nm.

The morphology of PZT nanoparticles was observed by TEM and HR-TEM micrographs, the particle size distribution was determined over 100 nanocrystals, being the average size 13.07 ± 2.81 nm (Fig. 2) which is in agreement with the average paricle size obtained from XRD pattern.

HR-TEM micrographs corroborate the formation of PZT nanoparticles, in Fig. 3, it can be observed a representative nanocrystal with dimension of 11.5 nm × 8.27 nm, with its electron diffraction pattern.

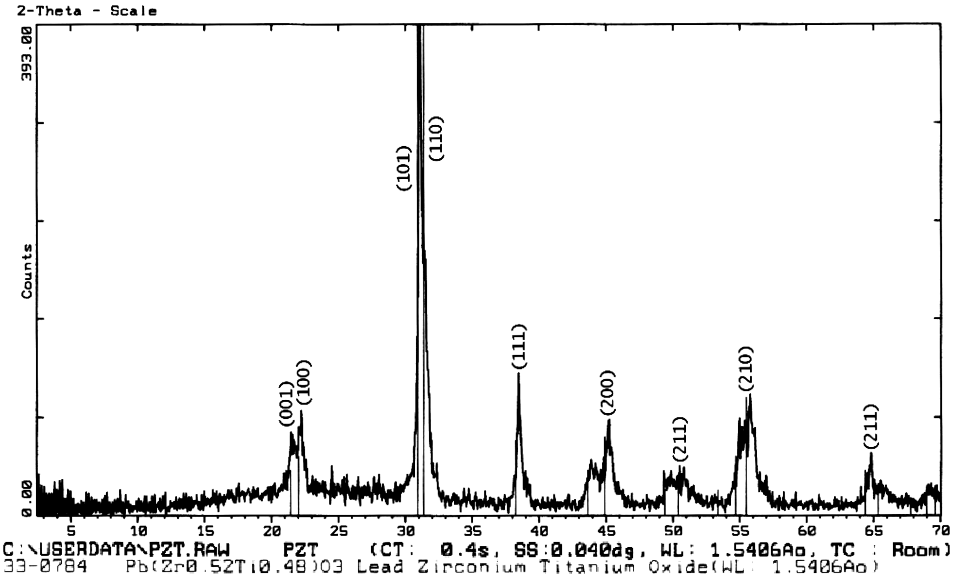

Figure 1. XRD pattern of Pb $(Zr_{0.52}Ti_{0.48})O_3$ nanoparticles.

3.2. Photoacoustic Experiments

In order to analyze the experimental photoacoustic response we constructed a correlation function as has been used previously [13–16], which reveals any change in the physical system under study. The correlation function is constructed considering the correlation between successive functions [PA(t, T_i)] and [PA(t, T_{i+1})], where PA(t, T_i) represents the interaction between the laser beam and the lattice, T_i describe different temperatures and the t index characterizes the size of the temporal signal. Physical instabilities can be revealed by

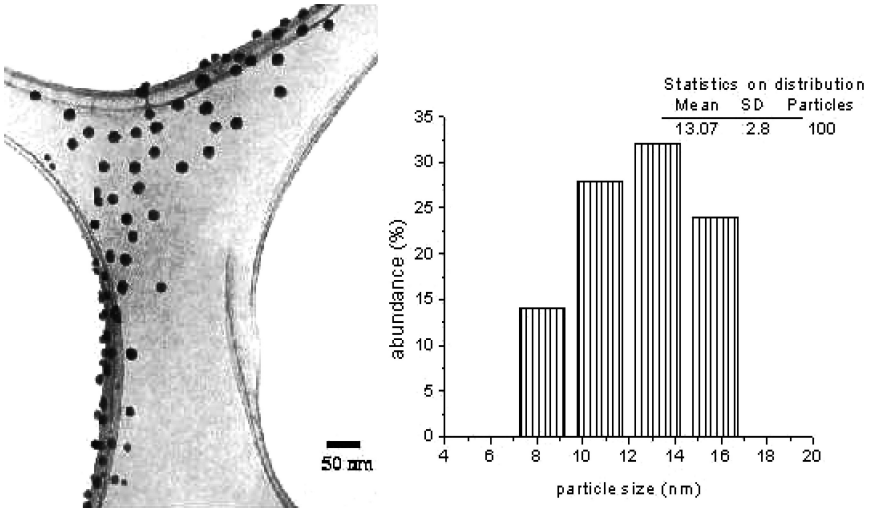

Figure 2. TEM micrograph and size distribution histogram of $Pb(Zr_{0.52}Ti_{0.48})O_3$ nanoparticles.

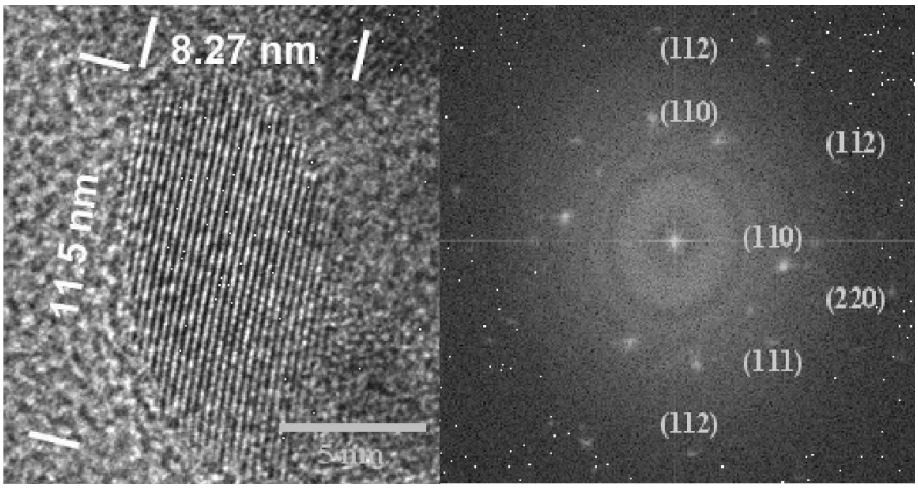

Figure 3. HRTEM micrograph and electron diffraction pattern of $Pb(Zr_{0.52}Ti_{0.48})O_3$ nanoparticles.

this correlation function since it shows any change of the temporal profile of the out coming acoustic pressure. Several photoacoustic experiments were carried out using different specimens, all of them performed at a heating rate so slow as to consider them temperature constant events. As a function of temperature, the curve in Fig. 4 stands for the out-going acoustic signal of a fresh powder sample.

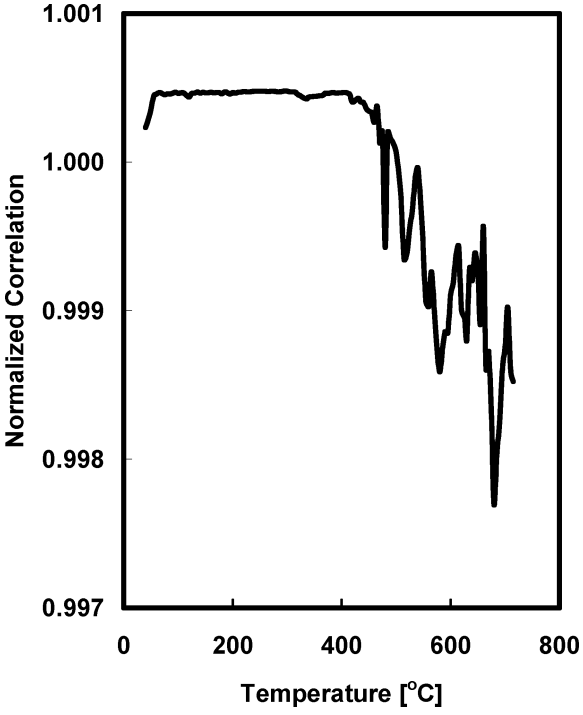

Figure 4. Stability photoacustic of $Pb(Zr_{0.52}Ti_{0.48})O_3$ nanocrystalline.

Usually, in a photoacoustic experiment performed with a bulk ceramic, the results obtained are repeatable. For a well-behaved ferroelectric transition, as that in $BaTiO_3$, the photoacoustic response at the transition temperature is a sharp peak [13], and a broad dispersive behavior is expected for a non classical ferroelectric transition [17]. This last resembling dielectric feature of relaxor ferroelectrics, whose resultant permittivity vs. T curve is a broad peak [18, 19]. In ferroelectric transition determination via photoacoustic experiments sintered samples are generally used. However, in an attempt to determine any characteristic temperature in as prepared nano-crystals, we have run a powdered sample. This in fact is the main reason why we used photoacoustic experiments in this research.

In the curve of Fig. 4 where are shown photoacoustic results for a powdered sample, a well-formed peak can be observed in the vicinity of 500°C, but beyond this temperature a very large dispersive behavior is also registered. Dispersion may be associated with relaxor behavior, but there are too many peaks in the curve, so experimental photoacoustic information seemed to be unintelligible in this case. Some arguments will be put forward in order to attempt explain that results. Curve in Fig. 5 announces the presence of instabilities which may be attributed to the size of the PZT-particles. As suggested in reference [20] physical properties of fine ferroelectric particles are affected via a surface tensional stress over the fine crystal surface due to the small radius of curvature. Under this point of view, crystal imperfections on the surface or even a tendency to force it back into the high symmetry phase can not be discarded. This physical situation could impede normal ferroelectric lattice behaviour. Then, since material was run as synthesized, the large temperature interval of instability (Fig. 5) may be attributed to a stage where regions at the grain boundaries tend to gradually eliminate defects and micro strain. Material evolves toward a stabilized system.

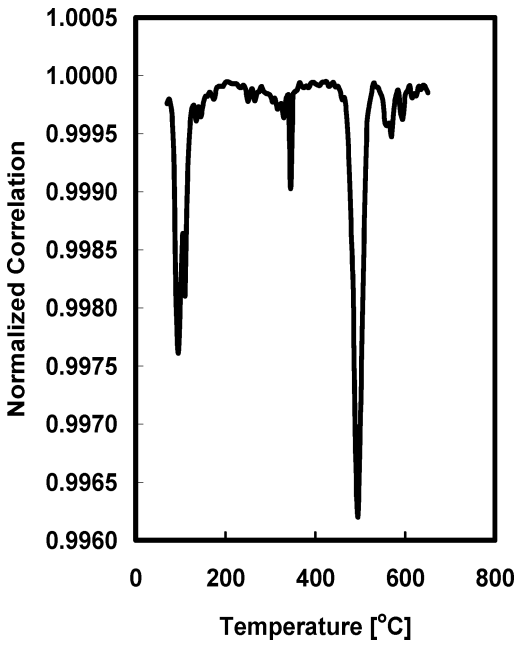

Figure 5. Effect of sintering on the temperature dependence of stability of Pb $(Zr_{0.52}Ti_{0.48})O_3$.

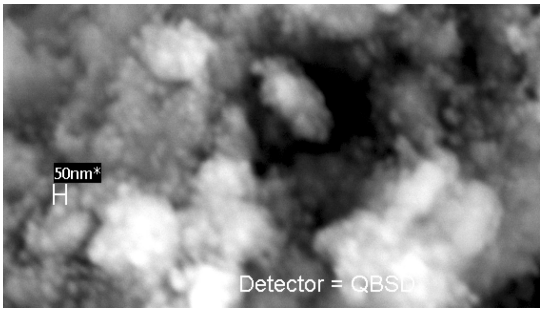

Figure 6. SEM image of sintered Pb $(Zr_{0.52}Ti_{0.48})O_3$. nanocrystals are forming large cumulus.

Besides, photoacoustic experiments were carried out in different powdered samples and the results always showed some differences. Nevertheless, in all experiments the presence of a peak close to 500°C was persistent. Therefore, it appears at first sight that there are difficulties drawing conclusions related to any characteristic temperature from this experiment. This compels us to perform experiments using sintered specimens, even when grain grow is unavoidable by the sintering process.

Figure 5 shows photoacoustic results of a sintered sample. Note the peak close to 500°C. There is also a small dispersion below 600°C, which is not comparable with that above 500°C in the curve of Fig. 4, then; sintered sample exhibit much more stability as a function of temperature. Successive experiments performed with the same sample, without any change in the experimental set up, showed some not significant differences, but resultant curves exhibited always the presence of the above mentioned broad peak close to 500°C. At this time, photoacoustic runs corresponds much more to a normal stable system, which exhibit a well located instability.

Regarding to the microstructure resulting from the sintering process, Fig. 6 shows a SEM image of the sintered sample. Specimen was prepared simply by fracturing the sample and a Cambridge-Leica Steroescan 440 scanning electron microscope was used to obtain microphotographs. Apparent large grains are formed by accumulation of nanoparticles. Since resolution at this level of image amplification is quite poor we only estimated that the average grain size is below 50 nm.

Particles are still in the nano range size. Heat treatment resulted in an increase in grain size, which is in average considerable larger than that for the starting nano powders. Changes influenced photoacoustic results, but the nature of the instability remains unclear. In the aim of clarifying the physical nature of the observed peak and using sintered samples we carried out dielectric experiments.

3.3. Dielectric Determinations

Dielectric experiments were performed from room temperature up to 660°C, however appropriate data to yield reliable information on dielectric features were obtained only above 300°C. Excitation with the ac field produces a semicircular response in the impedance plane, Fig. 7.

As can be observed, the curves are depressed towards the horizontal axis, which implies that a non Debye behaviour is present. There is no grain boundary effect on the electrical response. Therefore, data on the curve necessarily must be associated with the lattice dielectric

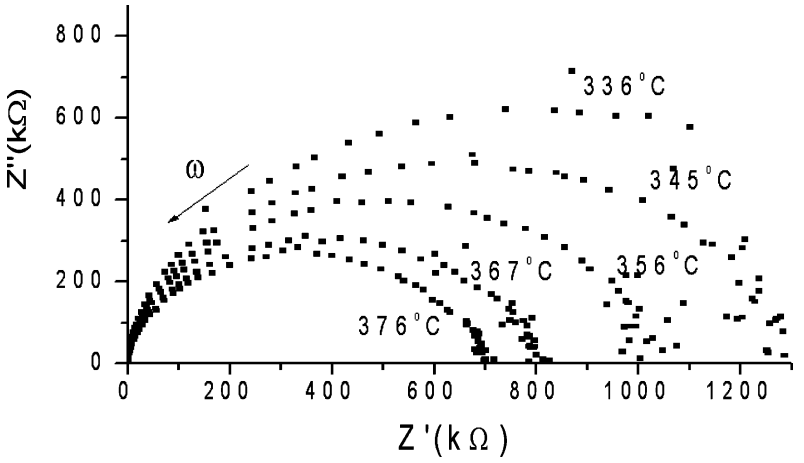

Figure 7. Typical impedance curves of sintered Pb $(Zr_{0.52}Ti_{0.48})\ O_3$.

behaviour. In principle, this offers the opportunity of obtaining lattice features directly by analyzing parameters extracted from the impedance curves, as has been reported [21–23]. This is, of course, an important point. A single RC parallel mesh would be an appropriate equivalent circuit. Under this model, at each temperature R values are diameters of semicircles. Also, at the top of each semicircle the relation $\omega_{max}RC = 1$ holds, where $\omega_{max} = 2\pi f_{max}$, and f_{max} is the measuring frequency. Therefore, using C values the dielectric constant, ε', can be straightforwardly obtained, since $\varepsilon' = gC/\varepsilon_o$, where g is a geometrical factor of the sample and $\varepsilon_o = 8.854\times10^{-14}$ F/cm is the vacuum dielectric constant.

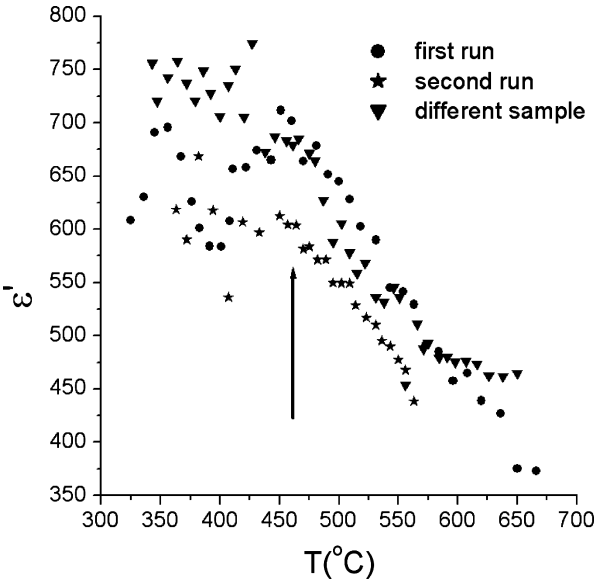

Figure 8. Frequency independent permittivity as a function of temperature of nanostructured PZT for sintered samples.

Figure 8 shows the temperature dependence of ε'. Results corresponds to three experiments, two of them performed with the same sample, with no change in the experimental set up, the other one performed with a different specimen.

Regarding the labeled "different sample" we point out that there is one experimental difference with respect to the sample which was measured twice; in the former case the sample was left for a longer time (more than a week) in the furnace when the dielectric data was acquired.

The technique selected to study this nano-system has been advantageously used to investigate bulky materials, however, as a function of temperature, the permittivity behavior of the nanostructured PZT shows a much more complex behavior than the expected one. A classical ferroelectric material produces a ε' against T curve which shows a sharp peak at the transition temperature, T_c. Furthermore, the shape of ε' vs. T curves, typical for a ferroelectric, usually are smooth, which is not the case for the studied materials (see Fig. 8). Probably, the sintering process has not yet completely eliminated anomalies at the grain surface. Further more, as suggested in reference [24], in nano compounds the grain size distribution may be affected by the occurrence of different shapes or morphologies that could alter the surface chemistry, presumably due to the presence of a number of defect sites per unit area, particularly related to the edge/corner relation. Then, we may expect that at least partially the dielectric properties would be influenced by those of the grain surface. Therefore, in principle the dielectric response of nanoparticles would differ from bulky behavior, mainly due to the different bonding geometry. At the end, the very complex dynamic atomic activity at the grain surface would mask the polarization activity of the ferroelectric state affecting the shape of the curve ε' vs. T, as happen in Fig. 8.

For curves in Fig. 8, there are some things to point out here; the first one is that the three curves show a discernible peak around 470°C. Besides, additional dispersion can be observed at temperatures above 470°C. Second, the dielectric constant of the samples is sensitive to the thermal treatment. Temperature dependence of ε' is very similar for fresh samples, whereas for the sample runs twice the corresponding ε' against T behaviour exhibit differences between different runs. These differences include those above 470°C, where the dielectric constant values for the first run are comparable to those corresponding to the second run. Furthermore, below the peak at 470°C, the curve for the different sample exhibits strong dispersion; this can also be noticed in the case of the curve for the second run. Incidentally, the largest calculated dielectric constant, observed in Fig. 8, lies below 800 in the three cases.

To have more elements to analyze, we worked out the temperature dependence of the dynamic dielectric parameter $\varepsilon'(\omega)$. In Fig. 9, as a function of temperature, we show results at 10 and 100 kHz of the first run from the sample which was run twice.

In this case the curves are quite smooth, but only an incipient hill is suggested at around 470°C. At lower frequencies and with the scale used in Figure 9 it will be very difficult to appreciate the presence of peaks on the corresponding curves.

From the same sample, curves corresponding to the first and second run, plotted at 1 MHz, are shown in Figure 10, they both exhibit a broad peak.

In the same figure curves for the different sample are also shown. In this last case the peak is shifted slightly toward low temperatures. Results related with the T_c, compare properly with those found in reference [25] where curves for nanocomposites of PZT ceramics shows a slope change at around 470°C, for the variation with temperature of dissipation factor.

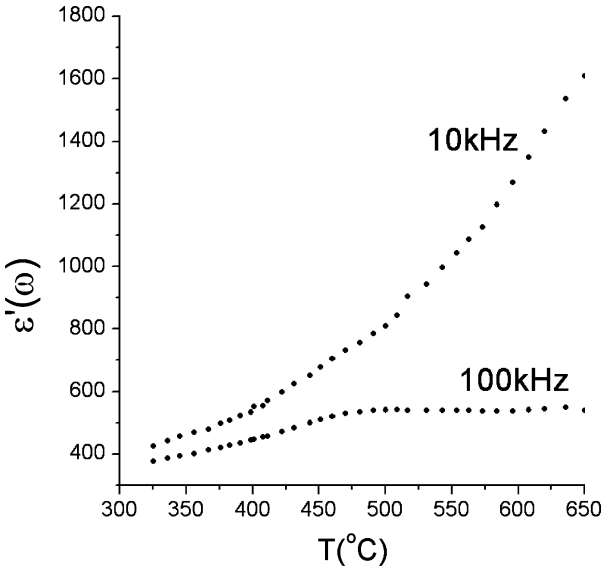

Figure 9. Dynamic permittivity as a function of temperature of Pb $(Zr_{0.52}Ti_{0.48})\ O_3$

At temperatures around T_c, in Fig. 11, we show the frequency dependence of the dynamic parameter $\varepsilon'(\omega)$. At low frequencies there is a strong dispersion, but as the frequency increases $\varepsilon'(\omega)$ tends to be frequency independent. The magnitude of $\varepsilon'(\omega)$ depends slightly on the temperature.

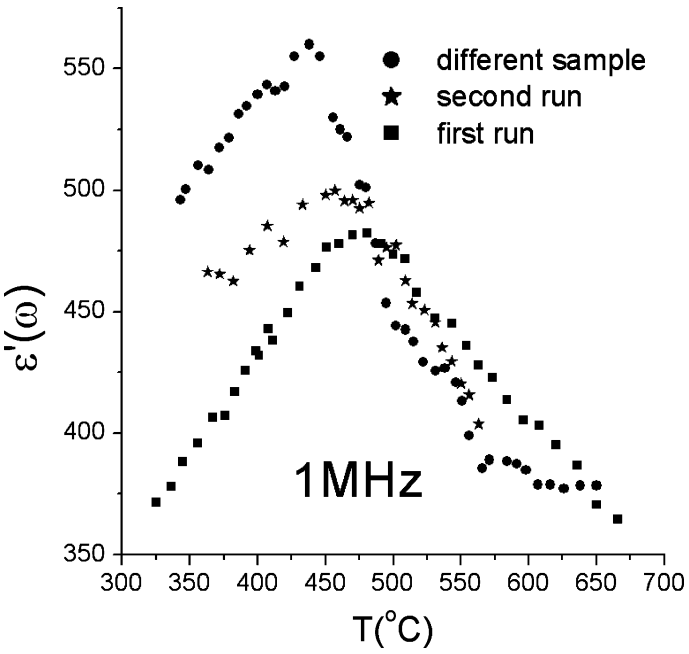

Figure 10. Dynamic permittivity at 1 MHz.

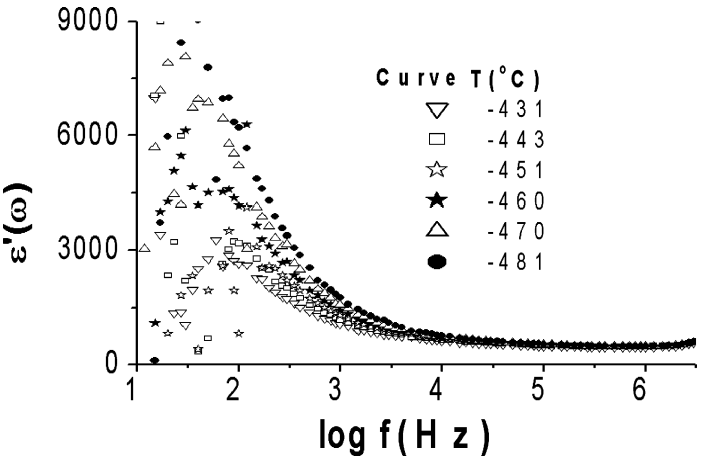

Figure 11. Frequency dependent behaviour of dynamic permittivity.

Then, finally there is no doubt on the existence of a transition temperature, although it seems to be dispersive in character. Regarding this last point, we believe that the material behaves as if it were constituted by a set of nano-ferroelectric grains, where ferroelectric domains would have a slightly different T_c. However, it seems to be difficult to classify the material behaviour as it were a relaxor, since there are difficulties to prove that Curie-Weis law fails or the maximum on the $\varepsilon'(\omega)$ vs. T curves is frequency dependent.

4. Conclusions

Using Sol-Gel method Pb $(Zr_{0.52}Ti_{0.48})O_3$ (PZT) nanostructured compounds have been synthesized. Crystallographic features were obtained by X-ray and electron microscopy techniques. The occurrence of a single phase was deduced from the X-ray diffraction data, whose peaks fit perfectly with a tetragonal structure. A combination of photoacoustic and dielectric techniques has proved to be appropriate to determine transition temperatures in the studied nanostructured samples. In earlier photoacoustic runs, using as synthesized fresh powders, large dispersion in a wide temperature interval was attributed to a no specific physical state, but anomalous, of the nano grain surface. Sintered material was then used to perform subsequent experiments, in which case both techniques were used as they normally are in dielectric bulky determinations. However unexpected results were still obtained in this case due to the presence of an unusual dispersive behavior with frequency and/or with temperature. Although the persistence of a peak below 500°C indicated that a characteristic temperature was involved. Using the very dedicated dielectric experiments reported here, it was finally stated that a transition occurs at around 470°C. The presence of excessive dispersion, in the curves of the frequency independent dielectric constant against temperature, must be due to instabilities at the surface of the nanograins, which masks the natural dipolar effect on the ferroelectric properties of the material. As a function of temperature, curves corresponding to the dynamic dielectric constant, $\varepsilon'(\omega)$, are much smoother than the corresponding to ε'. At low frequencies, plots of $\varepsilon'(\omega)$ against T reveal the presence of small hills at the transition temperature, but at high frequencies well-formed broad peaks are observed, especially at 1 MHz. Curves seem to be similar to those associated with a dispersive ferro-paraelectric transition, the maximum of which occurs close to 470°C.

Acknowledgments

Authors wish to thank CONACYT 44318 and PAPIIT IN114006 for financial support. Authors wish also to thank Dr. J. Guzmán Mendoza for helpful discussions, and to Fis. Raúl Reyes for technical support.

References

1. S. Choi, J. Heo, D. Kim, and I.Cheng, Ferroelectric properties of nano-size PZT grains determined by surface potential utilizing Kelvin force microscopy. *Thin Solid Films*. **464**, 277–281 (2004).
2. A. Abreu Jr., S. M. Zanetti, M. A. S. Oliveira, and G. P. Thim, Effect of urea on lead zirconate titanate Pb(Zr0.52 Ti0.48) O3 nanopowders synthesized by the Pechini method. *J. Eur. Ceram. Soc*. **25**, 743–748 (2005).
3. R. Ramesh, S. Aggarwal, and O. Auciello, Science and technology of ferroelectric films and heterostructures for non-volatile ferroelectric memories. *Mater. Sci. and Eng*. **32**, 191–236 (2001).
4. Paz de Araujo C. A: (Ed.) Proceedings of the 3–7th Internacional Simposium on Integrated Ferroelectrics. Colorado Springs: University of Colorado Press; 1991–1995.
5. S. Linardos, Q. Zhang, and J. R. Alcock, Preparation of sub-micron PZT particles with the sol-gel technique. *J. Eur. Ceram. Soc*. **26**, 117–123 (2006).
6. B. Jaffe, R. Cook, and H. Jaffe, Piezoelectric Ceramics. Academic Press, New York, 1971.
7. P. Duran and Moore, Piezoelectric ceramics. *Mater. Chem. Phys*. **15**, 193 (1986).
8. T. K. Kundu and D. Chakravorty, Nanocomposites of lead zirconate titanate glass ceramic and metallic silver. *Appl. Phys. Lett*. **67**(18), 2732–2734 (1995).
9. Y. Faheem and M. Shoaib, Sol-gel processing and characterization of phase pure lead zirconate titanate nano-powders. *J. Am. Ceram. Soc*. **89**(6), 2034–2037 (2006).
10. A. Fernández-Osorio, A. Vázquez-Olmos, E. Mata-Zamora, and J.M. Saniger, Preparation of free-standing $Pb(Zr_{0.52}Ti_{0.48})O_3$ nanoparticles by sol-gel method. *J. Sol-Gel Sci. and Tech. In press:* 2006.
11. H. Maiwa, O. Kimura, K. Shoji, and H. Ochiai, Low-Temperature Sintering of PZT Ceramics without additives via an ordinary ceramic route. *J. Eur. Ceram. Soc*. **25**, 2383–2391 (2005).
12. D. Damjanovic, S. S. N. Bharadwaja, and N. Setter, Toward a unified description of nonlinearity and frequency dispersion of piezoelectric and dielectric responses in Pb(ZrTi)O3. *Mater. Sci. and Eng*. **B120**, 170–174 (2005).
13. J. L. Pineda Flores, R. Castañeda-Guzmán, M. Villagrán Muniz, and A. Huanosta Tera, Ferro-paraelectric transitions in relaxor matrerials studied by a photoacoustic technique. *Apply. Phys. Lett*., **79**(8), 1166–1168 (2001).
14. R. Castañeda-Guzmán, M. Villagrán-Muniz, J. M. Saniger-Blesa, L. Lascano, and J. F. Fernández, Photoacoustic Study of Phase transition in Aurevilius Type Ceramics. *Ferroelectrics* **273**, 327–332 (2002).
15. R. Castañeda Guzmán, S. J. Pérez Ruíz, M. Villagrán Muñiz, and J. M. Saniger Blesa, Thermal Stability and Phase Transition by Photoacoustic Signal Analysis. *Analytical Science*. **17**, s122–s125 (2001).
16. R. Castañeda-Guzmán, M. Villagrán Muñiz, J. M. Saniger Blesa, S. J. Pérez-Ruiz, and O. Pérez-Martínez, Photoacoustic analysis of the ferroelectric ceramics specific heat. *Appl. Phys. Lett*. **77**(19), 3087–3089 (2000).
17. A. Huanosta-Tera, R. Castañeda-Guzmán, and L. Baños, M. Fernandez-Zamora, and M. Villagrán Muniz, Pulsed photoacoustic: A Realiable Technique to Investigate Diffuse Phase Transition and Associated Phenomena in Ferroelectrics, sent to Mater. *Res. Bull*. 2006.
18. L.E. Cross, Relaxor ferroelectrics: an overview. *Ferroelectrics*. **151**, 305 (1994).
19. I.-W. Chen and Y. Wang, Domain wall model for relaxor ferroelectrics. *Ferroelectrics*. **206–207**, 245–263 (1998).
20. K. Uchino, E. Sadanaga, and T. Hirose, Dependence of the Crystal Structure on Particle Size in Barium Titanate. *J. Am. Ceram. Soc*. **72**, 1555 (1989).

21. J. R. Mcdonald, Ed. Impedance Spectroscopy. John Wiley, New York; 1987.
22. A. K. Jonscher, Dielectric Relaxation in Solids (Chelsea Dielectric Press) London; 1983.
23. J. T. S. Irvine, D. C. Sinclair, and A. R. West, Electroceramics: Characterization. by ac Impedance Spectroscopy. *Adv. Mater.* **2**, 132–138 (1990).
24. K. J. Klabunde, Free Atoms, Clusters and Nanoscale Particles. Academic Press, San Diego; 1994.
25. T. K. Kundu and D. Chakravorty, Nanocomposites of lead-zirconate-titanate glass ceramics and metallic silver. *Appl. Phys. Lett.* **67**(18), 2732–2734 (1995).

Copyright of Ferroelectrics is the property of Taylor & Francis Ltd and its content may not be copied or emailed to multiple sites or posted to a listserv without the copyright holder's express written permission. However, users may print, download, or email articles for individual use.